ARTICLES

Collision-Energy-Resolved Penning Ionization Electron Spectroscopy of Nitriles: Conjugation Effects on Interactions with He*(2^3S) Metastable Atoms

Naoki Kishimoto, Johji Aizawa, Hideo Yamakado, and Koichi Ohno*

Department of Chemistry, Graduate School of Science, Tohoku University, Aoba-ku, Sendai 980-77, Japan

Received: October 28, 1996; In Final Form: February 17, 1997[⊗]

Penning ionization of propionitrile ($CH_3CH_2C{\equiv}N$), acrylonitrile ($CH_2{=}CHC{\equiv}N$), and 3-butenenitrile ($CH_2{=}CHCH_2C{\equiv}N$) upon collision with He*(2^3S) metastable atoms has been studied by two-dimensional Penning ionization electron spectroscopy in which Penning electron intensity is measured as a function of both collision energy and electron energy. We have observed a strong negative collision energy dependence of the partial ionization cross sections for ionization from nonbonding and π_{CN} orbitals of all samples studied, which indicates that the interaction potentials between He*(2^3S) and target molecules are strongly attractive around the cyano group. For π-conjugated acrylonitrile, strong attractive interaction was shown for the π_{CC} orbital region, while the attractive interaction for the π_{CC} orbital region became weak for nonconjugated 3-butenenitrile. The observed results are consistent with calculated model potential curves. The electron density difference for charge transfer was analyzed for the lone pair orbital region where the molecule acts as an electron donor, while the molecule acts as an electron acceptor for the conjugated π orbital region.

I. Introduction

A chemiionization process known as Penning ionization[1] can occur when a metastable atom A* collides with a target molecule (or atom) M, where A* has a larger excitation energy than the lowest ionization potential (IP) of M:

$$M + A^* \rightarrow M^+ + A + e^- \qquad (1)$$

Two important variables of this process: (a) collision energy E_c between A* and M in the entrance channel and (b) kinetic energy E_e of the ejected Penning electron in the exit channel, can be measured by (A) velocity (or collision energy) selection of A* and (B) Penning ionization electron spectroscopy,[2,3] respectively. Observed band intensities of Penning ionization electron spectra (PIES)[4] for various ionic states reflect partial ionization cross sections. One can, therefore, measure collision energy dependence of partial ionization cross sections (CEDPICS) by collision-energy-resolved Penning ionization electron spectroscopy[5−16] that is the combined technique of methods A and B.

When one measures total ionization cross sections as functions of collision energy, it is difficult to obtain information on anisotropic interaction potentials because the total ionization cross section, which is the sum of partial ionization cross sections, reflects averaged characteristics of the interaction potentials.[17−24] In the Penning ionization process, an electron in a molecular orbital (MO) having large electron densities outside the surface of M is transferred to the inner-shell orbital of A*, and the excited electron in A* is ejected.[25] It has been shown from the study[26] of partial ionization cross sections or branching ratios for Penning ionization that the most effective geometrical situations for the collisional ionization are different depending upon the electron distribution of the target MOs. Since the electron distribution of individual MOs is more or less localized on a special part of the molecule, the measurement of the CEDPICS for ionization from particular MOs enables us to obtain the local information on interaction potentials.

Recently, we have improved the efficiency of measurement by two methods:[27] (1) two-dimensional (2D) Penning ionization electron spectroscopy,[27a,28] which enables us to measure kinetic energies and time-dependent counts of Penning electrons simultaneously, and (2) the cross-correlation time-of-flight (TOF) method[27b,29] with a pseudorandom chopper for measuring the velocity distribution of A* and time-dependent distribution of Penning electrons. By combining these methods, it has become possible to measure collision-energy-resolved PIES (CERPIES) for various collision energies and CEDPICS for various electron energies at the same time with considerably improved signal-to-noise ratios of time-dependent counts.

In our previous studies,[7−16] we reported CERPIES and CEDPICS with one of the two variables of the Penning ionization process fixed, and we obtained information on the anisotropy of interaction potential for some molecules. Strong attractive potentials were shown in the pseudohalide terminal lone electron pair region of CH_3SCN,[11] CH_3CN,[14] and CH_3NC[14] with remarkably enhanced bands in PIES for nonbonding orbitals mainly localized on nitrogen or carbon atom (n_N or n_C), while the π orbital region of CH_3NCS[11] was shown to be more attractive than the n_S orbital region. Also, repulsive potentials were shown around the methyl group of these compounds. In this study, we investigated CEDPICS of propionitrile ($CH_3CH_2C{\equiv}N$), acrylonitrile ($CH_2{=}CHC{\equiv}N$), and 3-butenenitrile (arylcyanide: $CH_2{=}CHCH_2C{\equiv}N$) to elucidate the effect of the C=C bond and its distance from the C≡N group.

II. Experimental Section

We measured He*(2^3S) PIES and He I ultraviolet photoelectron spectra (UPS). For PIES, a metastable beam of He*(2^3S,2^1S) was produced by a discharge nozzle source[7−9] and

[⊗] Abstract published in *Advance ACS Abstracts,* June 15, 1997.

S1089-5639(96)03351-8 CCC: $14.00

the He*(2^1S) component was quenched by a water-cooled helium dc lamp. The He I resonance photons (21.22 eV) were produced by a discharge in pure helium gas. The energy resolution of the electron energy analyzer for the He*(2^3S) PIES and the He I UPS was estimated to be 60 meV. The transmission efficiency curve of the electron energy analyzer was determined by comparing UPS data with those by Gardner and Samson[30] and Kimura et al.[31]

In collision-energy-resolved Penning ionization electron spectroscopy, we have combined two techniques with the apparatus reported previously:[7−10] the 2D Penning ionization electron spectroscopy[27a,28] and the pseudorandom modulating cross-correlation TOF method.[27b,29] The metastable beam was pulsed by the pseudorandom chopper and introduced into a reaction cell located 504 mm downstream from the chopper disk. The pseudorandom chopper was made by etching two slit sequences of 127 elements on a 104-mm-diameter and 0.2-mm-thick brass disk. The element width of ca. 1.2 mm was selected to be comparable to the 1.0 mm diameter of the skimmer. Kinetic energies and time-dependent counts of emitted electrons from sample molecules or a reference stainless steel plate were analyzed by a hemispherical electron analyzer and stored in a 2 MB random-access memory (1M channels × 2 byte/channel). In 2D measurements, we lowered the resolution of the analyzer to 250 meV in order to obtain higher electron-counting rates. The time resolution Δt determined both by the rotational frequency (ca. 400 Hz) and the number of elements (2 × 127) was about 10 μs. Electron energies were scanned by 40 meV step, and a dwell time for the time-dependent measurement was 4 μs, which were both adequate for the electron energy and the time resolution.

The observed 2D electron intensity spectra $I_e(E_e,\tau)$ as a function of electron kinetic energy E_e and time τ (Figure 1a), which consisted of about 70 000 data points, were accumulated in about 6.5 h. The 2D spectra $I_e(E_e,\tau)$ were converted on a workstation to 2D spectra $I_e(E_e,\tau_{TOF})$ as a function of the time-of-flight of He* (Figure 1b) by Hadamard transformation in which time dependent signals were cross-correlated with the complementary sequence of the slit sequence. The $I_e(E_e,\tau_{TOF})$ can be led to $I_e(E_e,\nu_{He^*})$ as a function of the velocity of He* and then to the 2D Penning ionization cross section $\sigma(E_e,\nu_r)$ by the equations

$$\sigma(E_e,\nu_r) = c\{I_e(E_e,\nu_{He^*})/I_{He^*}(\nu_{He^*})\}(\nu_{He^*}/\nu_r) \quad (2)$$

$$\nu_r = [\nu_{He^*}{}^2 + 3kT/M]^{1/2} \quad (3)$$

where c is a constant, ν_r is the relative velocity averaged over the velocity of the target molecule, k is the Boltzmann constant, and T and M are the gas temperature and the mass of the target molecule, respectively. The origin of τ_{TOF} and velocity distribution of He* beam $I_{He^*}(\nu_{He^*})$ were determined by monitoring secondary electrons emitted from the inserted stainless plate. Finally, $\sigma(E_e,\nu_{He^*})$ is converted to the 2D-PIES $\sigma(E_e,E_c)$ by the relation

$$E_c = \mu\nu_r{}^2/2 \quad (4)$$

where μ is the reduced mass of the system (Figure 1c).

III. Calculations

We performed *ab initio* SCF calculations with 4-31G basis functions for neutral target molecules in order to obtain electron density contour maps, schematic diagrams of MOs, and orbital energies. The geometries of molecules were selected from literature for propionitrile,[32] acrylonitrile,[33] and 3-butenenitrile.[34]

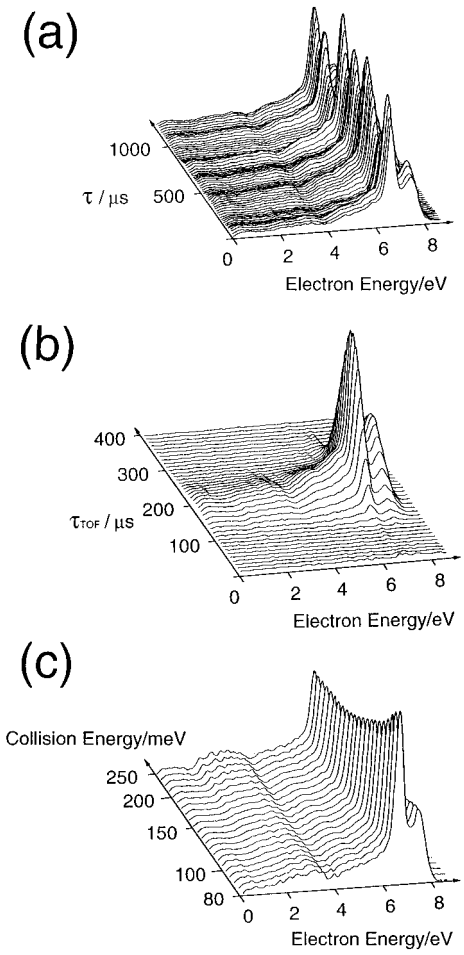

Figure 1. Schematic diagrams of 2D Penning ionization electron spectra for propionitrile: (a) observed 2D spectra $I_e(E_e,\tau)$ as a function of electron kinetic energy E_e and time τ, (b) converted 2D spectra $I_e(E_e,\tau_{TOF})$ as a function of E_e and the time-of-flight of He* τ_{TOF}, and (c) obtained 2D Penning ionization cross section $\sigma(E_e,E_c)$ as a function of E_e and collision energy E_c.

In electron density contour maps, thick solid curves indicate the repulsive molecular surface approximated by van der Waals radii.[35] In schematic diagrams of MOs, circles and ellipses were used. Solid circles showed valence s orbitals, where couples of ellipses and dashed circles showed in-plane and out-of-plane components of p orbitals, respectively.

Interaction potential energies between He*(2^3S) and M in various directions were also calculated on the basis of the well-known resemblance between He*(2^3S) and Li(2^2S); the shape of the velocity dependence of the total scattering cross section of He*(2^3S) by He, Ar, and Kr is very similar to that of Li,[36] and the location of the interaction potential well and its depth are similar for He*(2^3S) and Li with various targets.[17,18,37,38] Because of these findings and difficulties associated with calculations for excited states, the Li atom was used in this study in place of He*(2^3S). When we carried out interaction potential calculations for the out-of-plane direction of acrylonitrile with a 4-31++G** basis set, the calculations using an unrestricted Hartree−Fock (UHF) method and second-order Møller−Plesset perturbation (MP2) theory were difficult to converge or the obtained results were strongly spin contaminated. Then we calculated with density functional theory (DFT) for all M−Li systems in this study by the electron correlation energy correction taken in Becke's three-parameter exchange with the Lee, Young, and Parr correlation functional (B3LYP)[39] and checked the small degree of spin contamination by the expected values of the spin angular momentum. For comparison, the interaction energy values by MP2 or spin-projected MP2

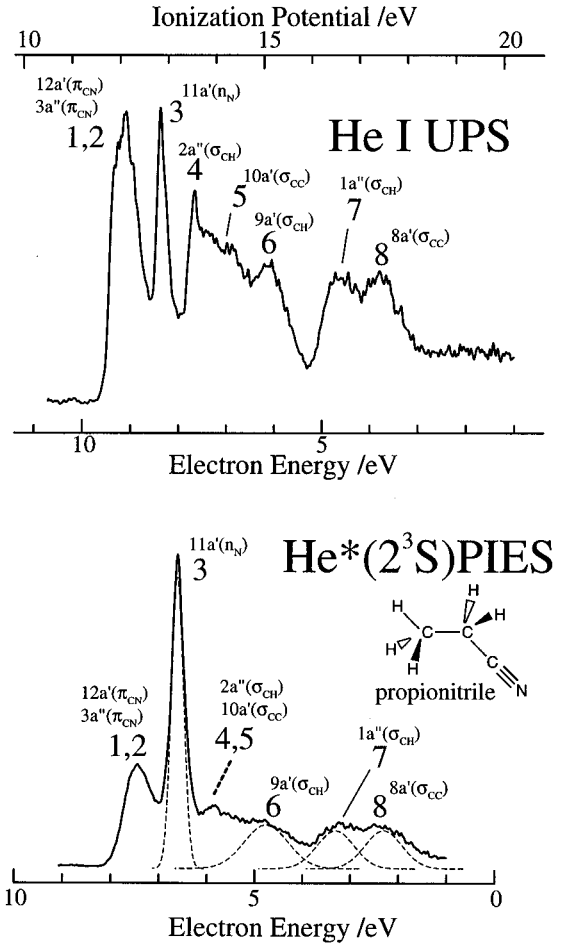

Figure 2. He I UPS and He*(2^3S) PIES of propionitrile.

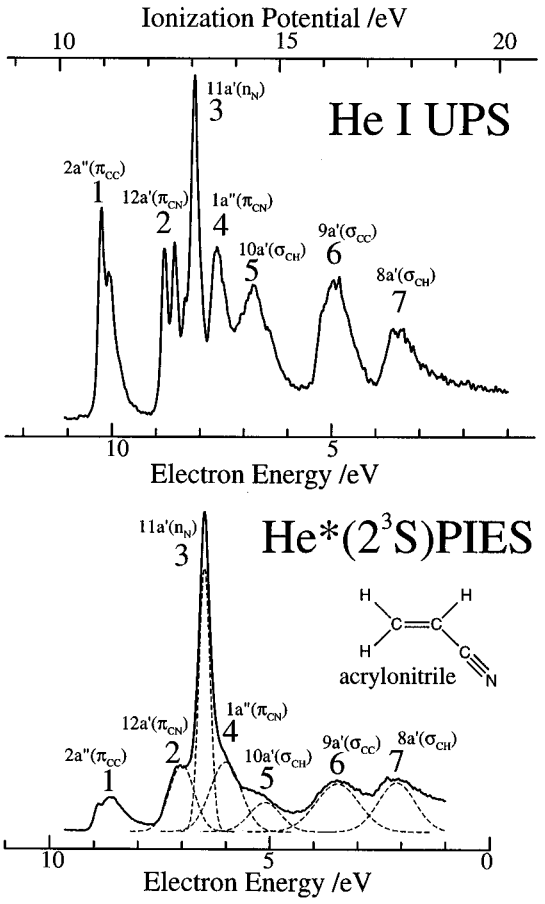

Figure 3. He I UPS and He*(2^3S) PIES of acrylonitrile.

(PMP2) calculations shall also be mentioned in this paper. All the calculations in this study were carried out by using a quantum chemistry program.[40]

In order to see the change of electron distribution upon charge transfer between the molecule and a lithium atom, the electron density difference was calculated with using wave functions obtained by DFT. In the electron density maps, the increase of electron density was plotted with solid lines and the decrease with dashed lines, respectively.

IV. Results

Figures 2−4 show the He I UPS and He*(2^3S) PIES of propionitrile, acrylonitrile, and 3-butenenitrile, respectively. The electron energy scales for PIES are shifted relative to those for the difference in the excitation energies, 21.22−19.82 = 1.40 eV. Some overlapping bands in PIES were decomposed into Gaussian type components and shown by dashed curves.

Figures 5−7 show the CERPIES of propionitrile, acrylonitrile, and 3-butenenitrile, respectively. In order to gain enough intensities, CERPIES were obtained from the 2D-PIES within ca. 20 μs width of TOF. In each figure, the low-collision-energy (ca. 90−110 meV, average 100 meV) spectrum is shown by a solid curve, the middle-collision-energy (ca. 135−165 meV, average 150 meV) spectrum is shown by a dotted curve, and the high-collision-energy (ca. 220−290 meV, average 250 meV) spectrum is shown by a dashed curve.

Figures 8−10 show the log σ vs log E_c plots of CEDPICS for propionitrile, acrylonitrile, and 3-butenenitrile, respectively. The CEDPICS were obtained from the 2D-PIES within an appropriate range of E_e (typically the fwhm of the respective band) to avoid the effect of neighboring bands. The calculated electron density maps of the molecular orbitals are also shown in the figures with simplified diagrams indicating component atomic orbitals. Electron density contour maps for σ orbitals are shown on the molecular plane, and those for π orbitals are shown on a plane at a height of 1.70 Å from the molecular plane.

Table 1 lists the vertical ionization potentials (IP determined from the He I UPS) and assignments of the observed bands. The peak energy shifts (ΔE) in PIES measured with respect to the "nominal" energy E_0 (E_0 = the difference between the metastable excitation energy and the target ionization potential) are also shown. The peak energy shifts to some diffuse bands or shoulders were not determined. Values of the slope parameter m for the log σ vs log E_c plots were estimated in a collision energy range for 150−185 meV by a least-squares method.

Figures 11−13 show model potential energy curves $V(R)$ by DFT (unrestricted B3LYP/4-31++G**) for propionitrile−Li, acrylonitrile−Li, and 3-butenenitrile−Li, respectively. The distance R between the target molecule and Li is measured from the nitrogen atom, the CN axis, or the molecular plane.

Figure 14 shows electron density difference contour maps of (a) propionitrile and Li for in-plane access along the CN bond axis (R = 2.0 Å), and acrylonitrile and Li for out-of-plane access to the vinyl group of (b) R = 3.0 Å and (c) R = 2.0 Å.

V. Discussion

A. Propionitrile. The UPS[31,41] as well as PIES[42] of propionitrile have been studied previously. In the PIES of propionitrile (Figure 2), an intense band 3 that originates from a lone pair n_N(11a′) orbital[43] shows large electron density exposed outside the molecular surface.[42] In this study, we observed a strong negative collision energy dependence of $\sigma(E_c)$ in CERPIES (Figure 5) and CEDPICS (Figure 8) for band

TABLE 1: Band Assignments, Ionization Potentials (IP/eV), Peak Energy Shifts (Δ*E*/meV), and Obtained Slope Parameter (*m*, See Text) for Nitriles

molecule	band	IP_{obsd}/eV	IP_{calcd}/eV	orbital character	Δ*E*/meV	*m*
propionitrile	1, 2	12.12	12.37	12a′(π_{CN})	−250 ± 100	−0.44 ± 0.09
			12.43	3a″(π_{CN})		
	3	12.83	14.56	11a′(n_N)	−390 ± 30	−0.50 ± 0.10
	4	13.55	14.73	2a″(σ_{CH})		−0.28 ± 0.07
	5	14.23	15.10	10a′(σ_{CC})		
	6	15.08	15.87	9a′(σ_{CH})	10 ± 100	−0.17 ± 0.12
	7	16.57	17.97	1a″(σ_{CH})	50 ± 100	0.10 ± 0.15
	8	17.40	19.05	8a′(σ_{CC})	−120 ± 100	−0.04 ± 0.12
acrylonitrile	1	10.97	10.62	2a″(π_{CC})	−230 ± 50	−0.30 ± 0.01
	2	12.63	12.72	12a′(π_{CN})	−190 ± 100	−0.41 ± 0.03
	3	13.07	14.84	11a′(n_N)	−270 ± 30	−0.60 ± 0.04
	4	13.60	14.10	1a″(π_{CN})	−220 ± 100	−0.47 ± 0.03
	5	14.42	15.70	10a′(σ_{CH})	−300 ± 200	−0.33 ± 0.03
	6	16.26	17.56	9a′(σ_{CC})	−110 ± 50	−0.12 ± 0.03
	7	17.75	19.58	8a′(σ_{CH})	30 ± 100	−0.11 ± 0.02
3-butenenitrile	1	10.60	10.47	3a″(π_{CC})	−20 ± 50	−0.10 ± 0.02
	2, 3	12.19	12.69	15a′(π_{CN})	−350 ± 100	−0.37 ± 0.01
			12.76	2a″(π_{CN})		
	4	12.98	14.97	13a′(n_N)	−350 ± 30	−0.48 ± 0.01
	5	13.40	14.20	14a′(σ_{CH})	−320 ± 100	(−0.32 ± 0.05)
	6	14.68	16.14	12a′(σ_{CC})	−120 ± 100	−0.07 ± 0.03
	7	15.93	17.46	1a″(σ_{CH})		0.02 ± 0.01
	8	16.35	17.90	11a′(σ_{CH},σ_{CC})		
	9	17.15	18.99	10a′(σ_{CH})	−50 ± 200	−0.03 ± 0.02
	10	19.26	21.65	9a′(C_{2s})		

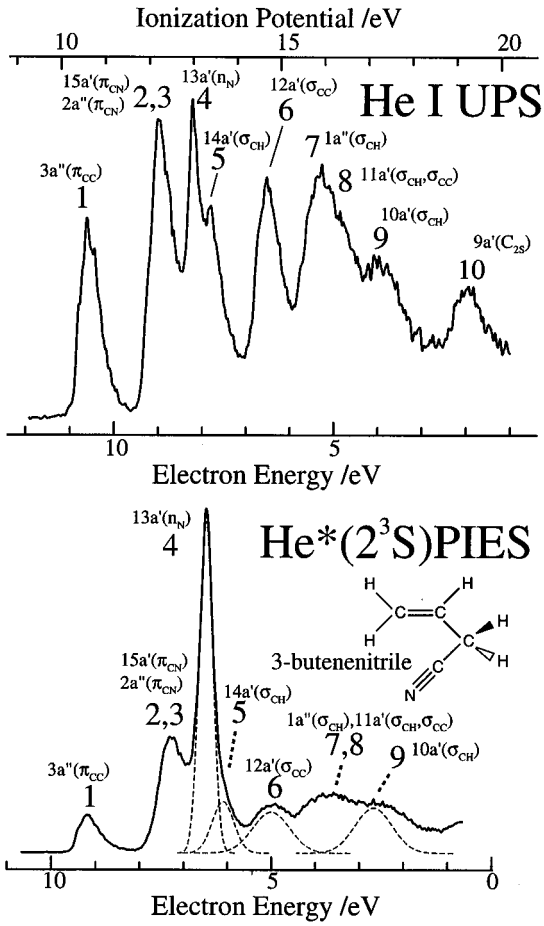

Figure 4. He I UPS and He*(2³S) PIES of 3-butenenitrile.

3 ($m = -0.50 \pm 0.10$). This negative dependence indicates that the potential energy surface of the entrance channel is strongly attractive along the CN bond axis. When the long-range attractive part of the interaction potential $V^*(R)$ plays a dominant role and its form is the type

$$V^*(R) \propto R^{-s} \tag{5}$$

we obtain the collision energy dependence of $\sigma(E_c)$ as

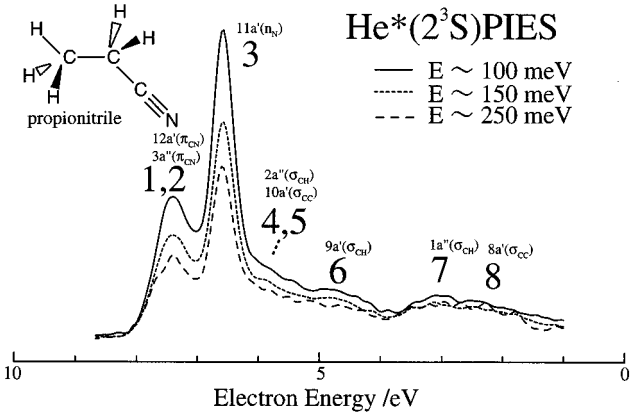

Figure 5. Collision-energy-resolved He*(2³S) PIES of propionitrile: solid curve at 93−108 meV, average 100 meV; dotted curve at 136−164 meV, average 150 meV; dashed curve at 223−284 meV, average 250 meV.

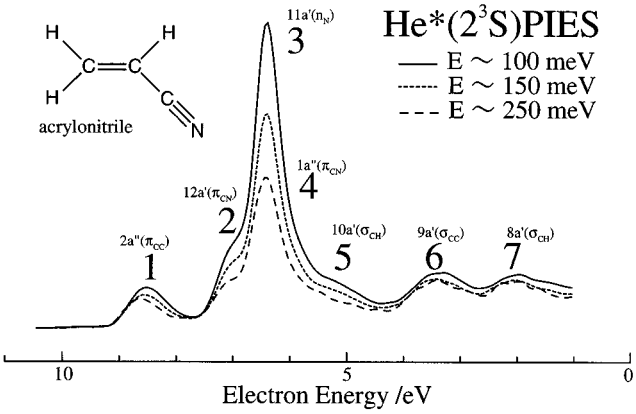

Figure 6. Collision-energy-resolved He*(2³S) PIES of acrylonitrile: solid curve at 92−110 meV, average 100 meV; dotted curve at 135−169 meV, average 150 meV; dashed curve at 217−300 meV, average 250 meV.

This equation gives a relationship between the slope parameter *m* and the potential parameter *s* ($m = -2/s$).[2,17,22] Indeed, an attractive potential curve with a deep well was calculated for straight access along the CN bond axis (Figure 11). In addition,

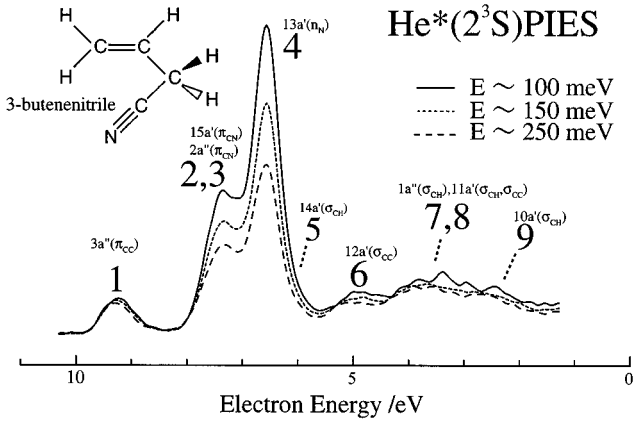

Figure 7. Collision-energy-resolved He*(2³S) PIES of 3-butenenitrile: solid curve at 92−111 meV, average 100 meV; dotted curve at 135−170 meV, average 150 meV; dashed curve at 218−294 meV, average 250 meV.

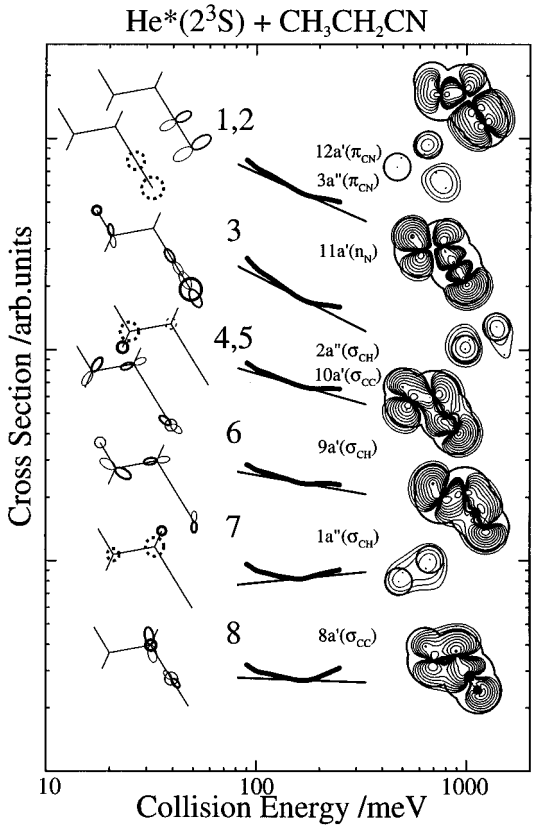

Figure 8. Collision energy dependence of partial ionization cross sections for propionitrile with He*(2³S).

a negative peak energy shift of band 3 ($\Delta E = -390 \pm 30$ meV) indicates the existence of an attractive potential well of this order, and the estimated value is in good agreement with the calculated value by DFT (ca. 400 meV) and an MP2 calculation (ca. 410 meV, $R = 2.0$ Å).

A strong negative collision energy dependence of band 1, 2 ($m = -0.44 \pm 0.09$) that originates from nearly degenerate π_{CN} orbitals also shows attractive potential for in-plane and out-of-plane directions around the CN bond. The calculated potential curve for out-of-plane access to the cyano group vertical to the molecular plane (Figure 11) shows a pulled-down shape with a shallow well (ca. 30 meV), which can indicate that a deep attractive potential well spreads widely around the n_N orbital region. The negative slope of CEDPICS for the π_{CN} bands can be ascribed to the effect of the strong attractive force. Comparing the observed results with the calculated results, the trends of steepness for anisotropic interaction potential curves are

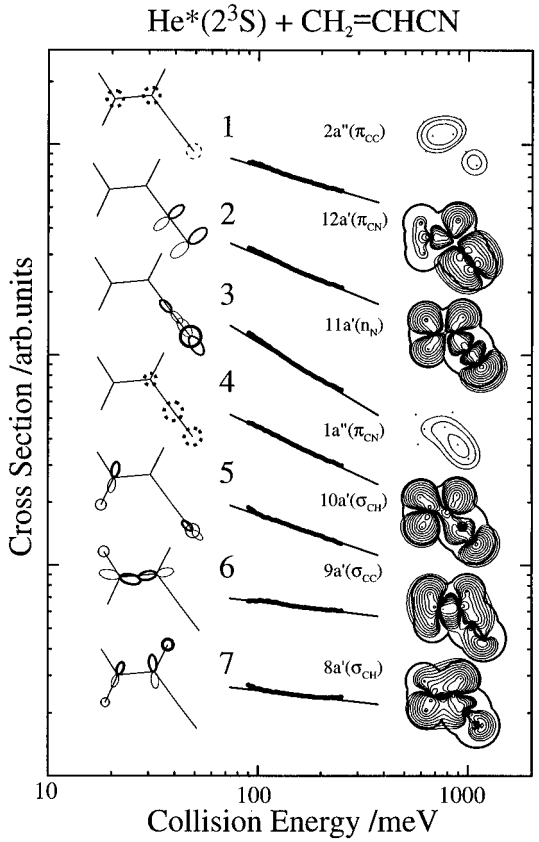

Figure 9. Collision energy dependence of partial ionization cross sections for acrylonitrile with He*(2³S).

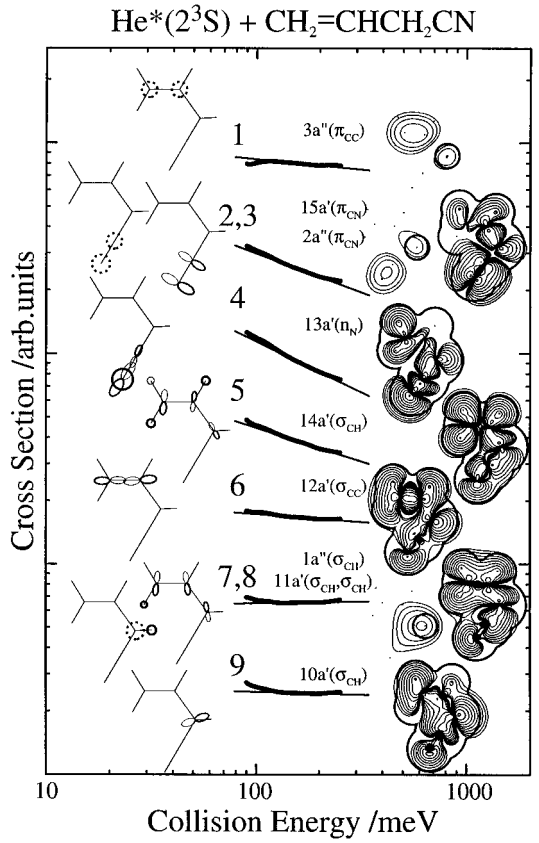

Figure 10. Collision energy dependence of partial ionization cross sections for 3-butenenitrile with He*(2³S).

consistent with obtained s values of n_N band ($s = 4.0$) and π_{CN} bands ($s = 4.5$). The strong attractive force can be connected with charge transfer from propionitrile to the lithium atom in the direction of the lone pair orbital as shown in the electron

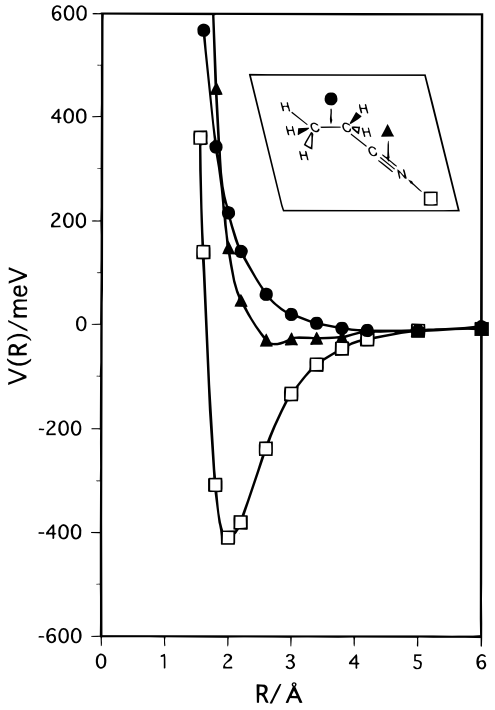

Figure 11. Model potential curves $V(R)$ for propionitrile−Li: (□) in-plane access along the CN axis; (▲) out-of-plane access vertical to the CN axis; (●) out-of-plane access to the ethyl group.

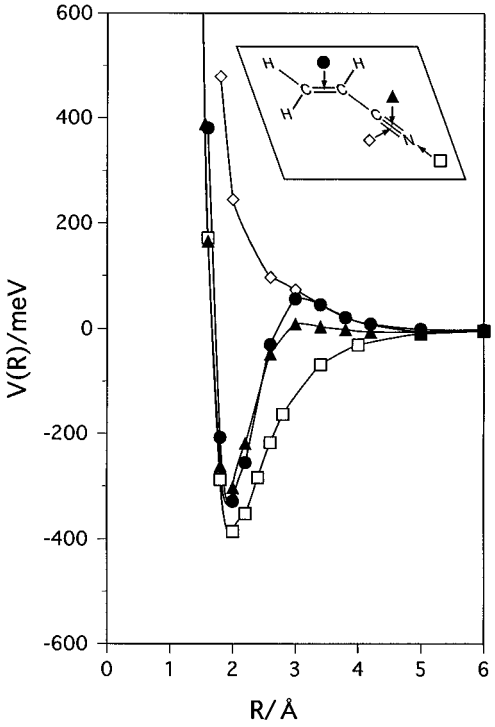

Figure 12. Model potential curves $V(R)$ for acrylonitrile−Li: (□) in-plane access along the CN axis; (◇) in-plane access vertical to the CN axis; (▲) out-of-plane access vertical to the CN axis; (●) out-of-plane access vertical to the vinyl group.

density difference map (Figure 14a), where the lithium atom acts as an electron acceptor by a 2s−2p hybridized orbital.

In contrast to the cases of the attractive potential, positive slope shown in the nonlinear behavior of band 7 (σ_{CH}) can be ascribed to a repulsive potential energy surface around the ethyl group. The calculated potential curve for out-of-plane access to the ethyl group shows a repulsive potential energy curve (Figure 11). As discussed in the literature,[8] when a repulsive term is dominant in the interaction, the slope parameter m is related to the parameters d and b by the equation $m = (b/d) - {}^1/_2$, where d is the effective decay parameter for the interaction potential between the target molecule and metastable atom ($V^*(R) = B \exp(-dR)$; R is the distance) and b is the effective parameter of the transition probability ($W(R) = C \exp(-bR)$) related to the IP of the molecule ($I(M)$) by the equation $b = 2\{2I(M)\}^{1/2}$. Similarly, the positive slope of nonlinear CED-PICS for band 8 can be ascribed to the 8a′(σ_{CC}) orbital whose density is distributed around the repulsive methylene region. For bands 4 and 5, the shape and position of each band were uncertain in PIES due to overlapping with band 6 or being hidden under the intense band 3 by its large negative peak shift ($\Delta E = -390 \pm 30$ meV). The negative slopes of band 4, 5 ($m = -0.28 \pm 0.07$) and band 6 ($m = -0.17 \pm 0.12$) can be ascribed to the relative large electron density of 10a′ and 9a′ orbitals around the cyano group, respectively.

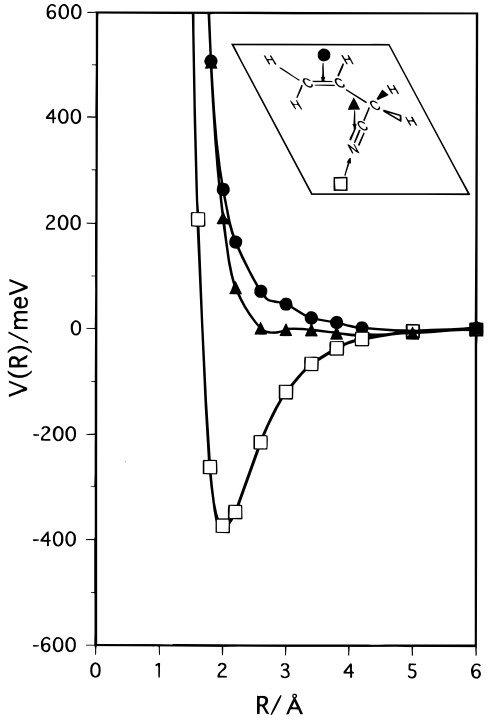

Figure 13. Model potential curves $V(R)$ for 3-butenenitrile−Li: (□) in-plane access along the CN axis; (▲) out-of-plane access vertical to the CN axis; (●) out-of-plane access vertical to the vinyl group.

B. Acrylonitrile. For the assignments of valence ionization spectra of acrylonitrile, extensive studies[31,41,42,44−51] have been investigated. It should be noted that the assignments of π_{CN} bands and n_N band were discussed[42,49] on the remarkable intensity of the n_N band in PIES (see Figure 3).

In this study, a strong negative collision energy dependence was observed (Figures 6 and 9) for the strongly enhanced n_N band ($m = -0.60 \pm 0.04$). The relatively small negative peak shift for the n_N band ($\Delta E = -270 \pm 30$ meV; $\Delta E = -210$ meV by Perreau et al.[49]) can be ascribed to a well of this order for the entrance channel, although the well depth was overestimated (Figure 12) by DFT (ca. 390 meV) and a PMP2 ($R =$ 2.0 Å, ca. 390 meV) calculation.

For an in-plane access to the cyano group, the π_{CN} band (band 2) showed weaker negative dependence ($m = -0.41 \pm 0.03$) than the n_N band ($m = -0.60 \pm 0.04$). This trend can also be explained by the influence of the strongly attractive CN bond region as for propionitrile, which is consistent with the negative peak shift ($\Delta E = -190 \pm 100$).

For out-of-plane directions of the conjugated π system, negative collision energy dependence was observed for the 2a″ (band 1, $m = -0.30 \pm 0.01$) and 1a″ (band 4, $m = -0.47 \pm 0.03$) orbitals. Since exterior electron density[26] outside the

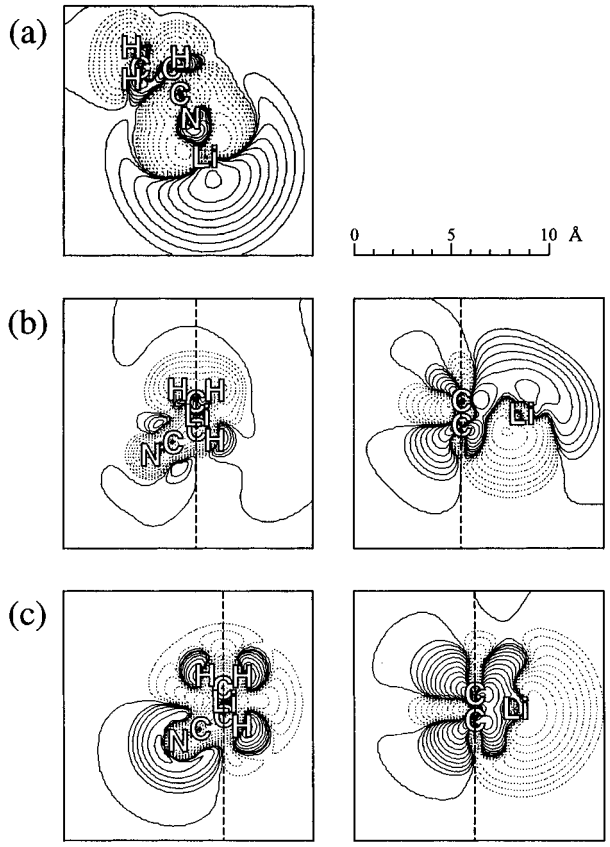

Figure 14. Electron density difference contour maps: (a) in-plane access along the CN axis ($R = 2.0$ Å) for propionitrile in the molecular plane; (b) out-of-plane access to the vinyl group ($R = 3.0$ Å) for acrylonitrile (the left panel is in the molecular plane; the right panel is in the vertical plane including the C═C bond and Li atom. The left panel and the right panel are intersecting each other along the dashed line); (c) out-of-plane access to the vinyl group ($R = 2.0$ Å) for acrylonitrile (the left panel is in the molecular plane; the right panel is in the vertical plane including the C═C bond and Li atom). The increase of electron is shown by solid lines, and the density difference of the nth solid line from the outside (d_n) is $2^{n-2} \times 10^{-5}$ au^{-3} except that d_1 is 0 au^{-3}. The decrease of electron is shown by dashed lines, and the density difference of the nth dashed line from the outside is $-2^{n-1} \times 10^{-5}$ au^{-3}.

$$\log \sigma(E_c) \propto (-2/s) \log E_c \qquad (6)$$

molecular surface is mostly localized on the vinyl group (69.2%) for the 2a″ orbital and on the CN group (70.0%) for the 1a″ orbital obtained by the SCF MO calculation, the negative dependence of band 1 and band 4 is expected to mainly reflect ionization in the π_{CC} and the π_{CN} regions, respectively. In contrast to the repulsive interaction around the ethyl group of propionitrile, the potential energy surface for out-of-plane access to the vinyl group of acrylonitrile is thought to be an attractive curve ($m = -0.30 \pm 0.01$, $s = 6.7$) steeper than in-plane access along the CN bond axis ($m = -0.60 \pm 0.04$, $s = 3.3$). The calculated potential curve by the DFT method shows an undulating attractive form that can be ascribed to curve crossing of two different electronic states in connection with the change of an occupied orbital from the 2s to 2p orbital of He*. The well depth is estimated from the negative peak shift ($\Delta E = -230 \pm 50$ meV), which is on the order of the calculated steep well of ca. 330 meV ($R = 2.0$ Å) by DFT. In PMP2 calculations, interaction potential energy for the out-of-plane access was increased to ca. +390 meV at $R = 2.2$ Å and then lowered to ca. +10 meV (ca. −70 meV for an optimized geometry) at $R = 2.0$ Å, which also suggests an undulating potential, but the potential barrier is too high for the collision energy range in this study. In the collision-energy-resolved PIES (Figure 6), the peak position of band 1 shifted to lower electron energy for lower collision energy spectra, which means that He* atoms of low collision energy are captured in the potential well and that the barrier height which is determined by centrifugal barrier and the hump of the potential curve is thought to be comparable with collision energy. The hump, therefore, should be smaller than +100 meV.

The calculated potential curve for out-of-plane access to the π_{CN} orbital region also shows a steep well by short-range attractive force, which is quite different from in-plane access to the cyano group (Figure 12). The stronger negative dependence of the π_{CN} band ($m = -0.47 \pm 0.03$) than that of the π_{CC} band ($m = -0.30 \pm 0.01$) is thought to reflect both the attractive force for the out-of-plane direction and the strong attractive force along the CN bond axis. The origin of the undulating attractive potential curve will be related with the π conjugation effect in section D.

Negative slopes for band 5 (σ_{CH}, $m = -0.33 \pm 0.03$), band 6 (σ_{CC}, $m = -0.12 \pm 0.03$), and band 7 (σ_{CH}, $m = -0.11 \pm 0.02$) are thought to be affected by the strong attractive force around the molecule, while the slope for the σ_{CH} band and σ_{CC} band of ethylene[13] gave positive values of ca. 0.12 and 0.18, respectively.

C. 3-Butenenitrile. The small slope of CEDPICS ($m = -0.10 \pm 0.02$) and the very small peak energy shift ($\Delta E = -20 \pm 50$ meV) of band 1 (π_{CC}) is consistent with a calculated repulsive interaction by DFT (Figure 13) and a PMP2 calculation ($R = 2.0$ Å, ca. +410 meV) for out-of-plane access to the π_{CC} orbital region, while attractive interaction was observed and calculated for the conjugated π_{CC} orbital region of acrylonitrile. From intensity ratio estimation of the π_{CC} and n_N bands ($I(\pi_{CC})/I(n_N)$) of acrylonitrile and 3-butenenitrile, the π_{CC} band of acrylonitrile (0.32) is enhanced compared with that of 3-butenenitrile (0.19), which also shows attractive interaction around the π_{CC} orbital region of acrylonitrile. As we shall mention in the next section, the effect of inserting a methylene group into the conjugated π_{CC} and π_{CN} system is thought to weaken the attractive force around the π_{CC} orbital region.

On the other hand, the potential energy around the cyano group is strongly attractive, which is shown by the CEDPICS and large negative peak energy shift of band 4 (n_N, $m = -0.48 \pm 0.01$, $\Delta E = -350 \pm 30$ meV) and nearly degenerate band 2, 3 (π_{CN}, $m = -0.37 \pm 0.01$, $\Delta E = -350 \pm 100$ meV). The experimental results are consistent with the trend of calculated curves by DFT (Figure 13). The slope of π_{CN} bands ($m = -0.37 \pm 0.01$) is similar to that for the nonconjugated in-plane π_{CN} orbital of acrylonitrile (band 2, $m = -0.41 \pm 0.03$).

The small collision energy dependence of band 6 (σ_{CC}, $m = -0.07 \pm 0.03$), band 7, 8 (σ_{CH}, σ_{CC}, $m = 0.02 \pm 0.01$), and band 9 (σ_{CH}, $m = -0.03 \pm 0.02$) can be ascribed to the repulsive σ_{CH} orbital region.

D. π Conjugation Effect. In electron density difference maps, large decrease of electron density between the lithium atom and acrylonitrile is shown for out-of-plane access to the π_{CC} orbital region of acrylonitrile at a distance of $R = 3$ Å (Figure 14b). On the contrary, a large increase of electron density both in the π_{CC} orbital region and around the cyano group by charge transfer from the electron-donating lithium atom is shown at a distance of $R = 2$ Å (Figure 14c), while charge transfers from the molecule to the lithium atom along the CN bond axis of propionitrile (Figure 14a). As discussed in a previous study,[46] the energy level of the lowest unoccupied molecular orbital (LUMO) of acrylonitrile is considerably lowered by both the inductively electron-withdrawing effect of the cyano group and the π conjugation effect of the π_{CN} and π_{CC} system for the out-of-plane direction. The lowered π^*-

type LUMO, therefore, can overlap with the 2p component of lithium atom in the short range as shown in the right panel of Figure 14c, which is thought to be the origin of the attractive force for the out-of-plane direction of acrylonitrile. In this connection, infrared and electron spin resonance spectroscopic studies[52,53] of $Li-CH_2CH_2$ complex showed π type equilibrium structure, which was confirmed to be a $^2B_2$ electronic ground state with a binding energy of ca. 2.2 kcal/mol (94 meV) by a DFT calculation[54] with geometry optimization. For some substituted ethylenes, on the other hand, a direct correlation between the energy levels of an occupied π_{CC} orbital and the slope of CEDPICS for π_{CC} bands has been observed.[55]

In contrast to a π-conjugated system, back-donation from He*(2^3S) to the LUMO of the sample molecule, which was mentioned above, cannot occur for a nonconjugated system because of higher energy of the LUMO. As mentioned above, the slope of the π_{CC} band became flattened from -0.30 ± 0.01 (acrylonitrile) to -0.10 ± 0.02 (3-butenenitrile) by inserting a methylene group into the conjugated π_{CC} and π_{CN} system, which is consistent with the peak energy shift of π_{CC} band for acrylonitrile ($\Delta E = -230 \pm 50$ meV) and for 3-butenenitrile ($\Delta E = -20 \pm 50$ meV).

VI. Conclusions

The partial ionization cross sections have shown characteristic negative collision energy dependence for propionitrile, acrylonitrile, and 3-butenenitrile by collision-energy-resolved Penning ionization electron spectroscopy, which indicates that the interaction potential between a He*(2^3S) metastable atom and the target molecule is highly anisotropic, having a repulsive potential around the σ_{CH} bond and an attractive potential around the lone pair orbital region around the nitrogen atom. Interaction potential curves by model calculation with Li(2^2S) instead of He*(2^3S) using DFT have been calculated and are in good agreement with the experimental results. The electron density difference has been analyzed for charge transfer from a molecule to the lithium atom in the direction of the lone pair orbital.

For a π-conjugated system, attractive potentials have been shown for out-of-plane access to the conjugated π orbital region by a strong negative collision energy dependence for the π_{CC} band and π_{CN} band, which can be explained by interorbital interactions of the 2p component of lithium atom with the energy-lowered π^*-type LUMO of acrylonitrile. By inserting a methylene group into the conjugated π_{CC} and π_{CN} system, the attractive force for the out-of-plane direction became weak in the nonconjugated system because of the higher energy of the LUMO than that of π-conjugated acrylonitrile.

Acknowledgment. This work has been supported by a Grant-in-Aid for Scientific Research from the Japanese Ministry of Education, Science, and Culture.

References and Notes

(1) Penning, F. M. *Naturwissenschaften* **1927**, *15*, 818.
(2) Niehaus, A. *Adv. Chem. Phys.* **1981**, *45*, 399.
(3) Yencha, A. J. *Electron Spectroscopy: Theory, Techniques, and Applications*; Brundle, C. R., Baker, A. D., Eds.; Academic: New York, 1984; Vol. 5.
(4) Čermák, V. *J. Chem. Phys.* **1966**, *44*, 3781.
(5) Dunlavy, D. C.; Martin, D. W.; Siska, P. E. *J. Chem. Phys.* **1990**, *93*, 5347.
(6) Longley, E. J.; Dunlavy, D. C.; Falcetta, M. F.; Bevsek, H. M.; Siska, P. E. *J. Phys. Chem.* **1993**, *97*, 2097.
(7) Mitsuke, K.; Takami, T.; Ohno, K. *J. Chem. Phys.* **1989**, *91*, 1618.
(8) Ohno, K.; Takami, T.; Mitsuke, K.; Ishida, T. *J. Chem. Phys.* **1991**, *94*, 2675.
(9) Takami, T.; Mitsuke, K.; Ohno, K. *J. Chem. Phys.* **1991**, *95*, 918.
(10) Takami, T.; Ohno, K. *J. Chem. Phys.* **1992**, *96*, 6523.
(11) Pasinszki, T.; Yamakado, H.; Ohno, K. *J. Phys. Chem.* **1993**, *97*, 12718.
(12) Ohno, K.; Kishimoto, N.; Yamakado, H. *J. Phys. Chem.* **1995**, *99*, 9687.
(13) Ohno, K.; Okamura, K.; Yamakado, H.; Hoshino, S.; Takami, T.; Yamauchi, M. *J. Phys. Chem.* **1995**, *99*, 14247.
(14) Pasinszki, T.; Yamakado, H.; Ohno, K. *J. Phys. Chem.* **1995**, *99*, 14678.
(15) Yamakado, H.; Yamauchi, M.; Hoshino, S.; Ohno, K. *J. Phys. Chem.* **1995**, *99*, 17093.
(16) Kishimoto, N.; Yamakado, H.; Ohno, K. *J. Phys. Chem.* **1996**, *100*, 8204.
(17) Illenberger, E.; Niehaus, A. *Z. Phys. B* **1975**, *20*, 33.
(18) Parr, T. P.; Parr, D. M.; Martin, R. M. *J. Chem. Phys.* **1982**, *76*, 316.
(19) Pesnelle, A.; Watel, G.; Manus, C. *J. Chem. Phys.* **1975**, *62*, 3590.
(20) Woodard, M. R.; Sharp, R. C.; Seely, M.; Muschlitz, E. E., Jr. *J. Chem. Phys.* **1978**, *69*, 2978.
(21) Appolloni, L.; Brunetti, B.; Hermanussen, J.; Vecchiocattivi, F.; Volpi, G. G. *J. Chem. Phys.* **1987**, *87*, 3804.
(22) Allison, W.; Muschlitz, E. E., Jr. *J. Electron Spectrosc. Relat. Phenom.* **1981**, *23*, 339.
(23) Riola, J. P.; Howard, J. S.; Rundel, R. D.; Stebbings, R. F. *J. Phys. B* **1974**, *7*, 376.
(24) Lindinger, W.; Schmeltekopf, A. L.; Fehsenfeld, F. C. *J. Chem. Phys.* **1974**, *61*, 2890.
(25) Hotop, H.; Niehaus, A. *Z. Phys.* **1969**, *228*, 68.
(26) Ohno, K.; Mutoh, H.; Harada, Y. *J. Am. Chem. Soc.* **1983**, *105*, 4555.
(27) (a) Ohno, K.; Yamakado, H.; Ogawa, T.; Yamata, T. *Int. Conf. Phys. Electron. At. Collisions, 19th, 1995* **1995**, 413. (b) Kishimoto, N.; Yamakado, H.; Yamata, T.; Ogawa, T.; Ohno, K. *Int. Conf. Phys. Electron. At. Collisions, 19th, 1995* **1995**, 807.
(28) Ohno, K.; Yamakado, H.; Ogawa, T.; Yamata, T. *J. Chem. Phys.* **1996**, *105*, 7536.
(29) Auerbach, D. J. *Atomic and Molecular Beam Methods*; Scoles, G., Ed.; Oxford University: New York, 1988; p 369.
(30) Gardner, J. L.; Samson, J. A. R. *J. Electron Spectrosc. Relat. Phenom.* **1976**, *8*, 469.
(31) Kimura, K.; Katsumata, S.; Achiba, Y.; Yamazaki, T.; Iwata, S. *Handbook of He I Photoelectron Spectra of Fundamental Organic Molecules*; Japan Scientific: Tokyo, 1981.
(32) Lerner, R. G.; Dailey, B. P. *J. Chem. Phys.* **1957**, *26*, 678.
(33) Fukuyama, T.; Kuchitsu, K. *J. Mol. Struct.* **1970**, *5*, 131.
(34) Schei, S. H. *J. Mol. Struct.* **1983**, *98*, 141.
(35) Pauling, L. *The Nature of the Chemical Bond*; Cornell University: Ithaca, NY, 1960.
(36) Rothe, E. W.; Neynaber, R. H.; Trujillo, S. M. *J. Chem. Phys.* **1965**, *42*, 3310.
(37) Hotop, H. *Radiat. Res.* **1974**, *59*, 379.
(38) Haberland, H.; Lee, Y. T.; Siska, P. E. *Adv. Chem. Phys.* **1981**, *45*, 487.
(39) Becke, A. D. *J. Chem. Phys.* **1993**, *98*, 5648.
(40) Frisch, C. M. J.; Trucks, G. W.; Head-Gordon, M.; Gill, P. M.; Wong, M. W.; Foresman, J. B.; Johnson, B. G.; Schlegel, H. B.; Robb, M. A.; Replogle, E. S.; Gomperts, R.; Andres, J. L.; Raghavachari, K.; Binkley, J. S.; Gonzalez, C.; Martin, R. L.; Fox, D. J.; Defrees, D. J.; Baker, J.; Stewart, J. J. P.; Pople, J. A. *Gaussian 92/DFT*; Gaussian, Inc.: Pittsburgh, PA, 1992.
(41) Lake, R. F.; Thompson, H. *Proc. R. Soc. London A.* **1970**, *317*, 187.
(42) Ohno, K.; Matsumoto, S.; Imai, K.; Harada, Y. *J. Phys. Chem.* **1984**, *88*, 206.
(43) The lone pair orbital or nonbonding orbital of the CN group was denoted as the n_N orbital as in ref 42, whereas this type of orbital was referred to as a σ_{CN} orbital in ref 31.
(44) Moffat, J. B.; Collens, R. J. *J. Mol. Spectrosc.* **1968**, *27*, 252.
(45) Baybutt, P.; Guest, M. F.; Hiller, I. H. *Mol. Phys.* **1973**, *25*, 1025.
(46) Houk, K. N.; Munchausen, L. L. *J. Am. Chem. Soc.* **1976**, *98*, 937.
(47) Stafast, H.; Bock, H. *Tetrahedron* **1976**, *32*, 855.
(48) Bieri, G.; Åsbrink, L.; von Niessen, W. *J. Electron Spectrosc. Relat. Phenom.* **1982**, *27*, 129.
(49) Perreau, J.; Reynaud, C.; Lécayon, G.; Ellinger, Y. *J. Phys. B: At. Mol. Phys.* **1986**, *19*, 1497.
(50) von Niessen, W.; Cambi, R. *Chem. Phys.* **1986**, *103*, 11.
(51) Delwiche, J.; Gochel-Dupuis, M.; Collin, J. E.; Heinesch, J. *J. Electron Spectrosc. Relat. Phenom.* **1993**, *66*, 65.
(52) Manceron, L.; Andrews, L. *J. Phys. Chem.* **1986**, *90*, 4514.
(53) Manceron, L.; Schrimpf, A.; Bornemann, T.; Rosendahl, R.; Faller, F.; Stöckmann, H.-J. *Chem. Phys.* **1993**, *169*, 219.
(54) Alikhani, M. E.; Hannachi, Y.; Manceron, L.; Bouteiller, Y. *J. Chem. Phys.* **1995**, *103*, 10128.
(55) (a) Okamura, K. M.Sc. Thesis, Tohoku University, 1995. (b) Yamakado, H.; Okamura, K.; Ohshimo, K.; Kishimoto, N.; Ohno, K. *Chem. Lett.* **1997**, 269.